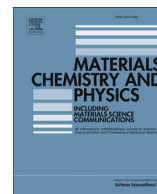




Contents lists available at ScienceDirect

Materials Chemistry and Physics

journal homepage: www.elsevier.com/locate/matchemphys

Morphology-controllable synthesis and characterization of carbon nanotube/polypyrrole composites and their hydrogen storage capacities

Burcu Saner Okan ^{a,*}, Jamal Seyyed Monfared Zanjani ^b, Ilse Letofsky-Papst ^c,
Fevzi Çakmak Cebeci ^{a,b}, Yusuf Z. Menceloglu ^{a,b}

^a Sabancı University Nanotechnology Research and Application Center, SUNUM, Tuzla, Istanbul 34956, Turkey

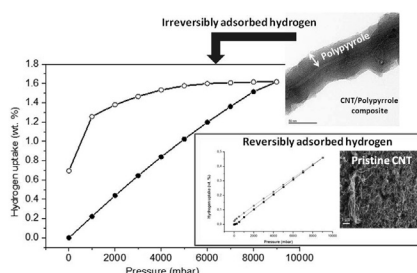
^b Faculty of Engineering and Natural Sciences, Sabancı University, Tuzla, Istanbul 34956, Turkey

^c Institute for Electron Microscopy, Graz University of Technology, Steyrergasse 17, A-8010, Graz, Austria

HIGHLIGHTS

- Growth mechanisms of polypyrrole are controlled by changing monomer concentration.
- Lamellar structure is formed by using pristine CNT at high monomer concentration.
- Homogeneous polymer coating is achieved on the surface of oxidized CNT.
- CNT/polypyrrole composite has the highest hydrogen adsorption capacity (1.66 wt%).
- Polymer coating and chemical oxidation affects hydrogen sorption isotherms.

GRAPHICAL ABSTRACT



ARTICLE INFO

Article history:

Received 15 February 2015

Received in revised form

31 August 2015

Accepted 11 October 2015

Available online xxx

Keywords:

Composite materials

Oxidation

Polymers

Surface properties

Adsorption

Desorption

ABSTRACT

Sphere-like and layer-by-layer growth mechanisms of polypyrrole are controlled by changing pyrrole monomer concentration and using carbon nanotubes (CNT) as template. Pristine polypyrrole has sphere-like structures but remarkable change in types of polypyrrole growth is observed from spherical-like to layer-by-layer structures in the presence of CNT. Acid treatment enhances polypyrrole coverage on CNT surface by preventing agglomeration of polypyrrole due to an increase in surface oxygen groups and sp^2 bonds in CNT structure. The crystallinity of powders comparably decreases after polypyrrole coating due to the amorphous structure of polypyrrole and a sharp decrease in the intensity of 002 peak. The influence of surface functionalization and polymer coating on the structural parameters of multi-walled CNT and their composites is investigated by tailoring the feeding ratio of pyrrole. The hydrogen sorption measurements at ambient conditions by Intelligent Gravimetric Analyzer demonstrate that hydrogen uptake of CNT/polypyrrole composite is 1.66 wt.% which is almost 3 times higher than that of pristine CNT. Higher hydrogen uptake values are obtained by keeping the mass ratio of pyrrole monomer and CNT equal by using non-functionalized CNT in composite production. Hydrogen adsorption/desorption kinetics of polypyrrole/CNT composites is improved by increasing adsorption sites after

* Corresponding author.

E-mail address: bsanerokan@sabanciuniv.edu (B.S. Okan).

different feeding ratios of Py. The feeding mass ratios of Py and MWCNT were 1:1 and 2:1.

2.4. Measurement of hydrogen storage capacity

Hydrogen adsorption measurements were performed by Hiden Isochema 001 Intelligent Gravimetric Analyzer (IGA) at room temperature under 9000 mBar pressure. CNT and its composites were outgassed for 24 h at room temperature.

2.5. Characterization

The layer thickness and the surface of CNT and their composites were analyzed by a Leo Supra 35VP Field Emission Scanning Electron Microscope (SEM) by using secondary electron and inlens detectors and JEOL 2100 Lab6 High Resolution Transmission Electron Microscopy (TEM). The degree of oxidation and the ratio of C, O and N ratios were estimated by Electron Energy Loss Spectroscopy (EELS). X-ray diffraction (XRD) measurements were conducted by a Bruker AXS advance powder diffractometer fitted with a Siemens X-ray gun, using $\text{CuK}\alpha$ radiation ($\lambda = 1.5406 \text{ \AA}$). Crystallite size in composites was calculated by using the classical Debye–Scherrer equations:

$$L_a = 0.89\lambda/\beta_{002} \cos \theta_{002}$$

where L_a is the stacking height and β is the full width half maxima (FWHM). Crystallite size in polymers is generally in nano-scale and in the thickness direction. Structural changes of MWCNT were investigated by Renishaw InVia Reflex Raman Microscopy System using (Renishaw Plc., New Mills, Wotton-under-Edge Gloucestershire, UK) using a 514 nm argon ion laser in the range of 100–3200 cm^{-1} . The functional groups of composites were determined by Netzsch Fourier Transform Infrared Spectroscopy (FTIR). The specific surface area of samples was measured by Quantachrome NOVA 2200e series Surface Analyzer by the Brunauer–Emmett–Teller (BET) method in the P/P0 range of 0.05–0.35. All samples were outgassed for 24 h at 150 °C. The pore size distribution was obtained from the desorption isotherms using the Barrett–Joyner–Halenda (BJH) method.

3. Results and discussion

3.1. Synthesis of PPy/CNT composites

In the first stage, non-functionalized MWCNT surface is coated by PPy with different weight ratios of pyrrole monomer to observe the structural changes. XRD characterization results show that PPy is amorphous polymer. After the coverage of functionalized CNT with different feeding ratios of PPy, the intensity of a crystalline peak of CNT corresponding to the (002) reflection at around $2\theta = 26.5^\circ$ decreases and the peak broadens (Fig. 2). The structure of CNT based composites becomes more amorphous by increasing PPy content and thus the crystallinity significantly decreases.

The structural change is also observed by comparing the intensity ratios of D and G bands, I_D/I_G , in Raman spectra of CNT samples. These bands are observable in all poly-aromatic hydrocarbons. I_D/I_G ratio directly changes with the size of the crystalline grains or interdefect distance [30]. Also, I_D/I_G ratio is related to the atomic ratio of sp^2/sp^3 that is a measure of the extent of disordered graphitic structure [31]. Fig. 3 represents the Raman spectra of pristine CNT, Py:CNT = 1:1 and Py:CNT = 2:1. As the feeding mass ratio of Py to CNT increases in powders, D and G bands start to combine each other since the amorphous structure of PPy directly decreases the crystallinity of CNT. Table 1 gives the intensities of D

and G bands, and the changes in I_D/I_G ratios of pristine CNT, Py:CNT = 1:1 and Py:CNT = 2:1 composites. The I_D/I_G ratio decreases slightly as the polymer concentration increases. This shows that polymers are bonded noncovalently onto nanotube surface and thus the degree of disorder of CNT does not change significantly. In addition, the disappearance of 2D peak after PPy coating indicates the formation of amorphous structure [32].

Fig. 4 represents FTIR spectra of pristine CNT, PPy, Py:CNT = 1:1 and Py:CNT = 2:1 composites. There was no observable peak in FTIR spectrum of pristine CNT due to its high carbon content and strong C–C bonds. In FTIR spectrum of pure PPy, the peak at 1555 cm^{-1} is corresponded to the C–C stretching vibrations and the peak at 926 cm^{-1} is due to C–N wagging vibration of Py ring [33]. Also, the peaks at 1050 cm^{-1} and 1197 cm^{-1} are attributed to C–H in-plane deformation vibration of PPy and the breathing vibration of the pyrrole ring, respectively [33]. On the other hand, only the characteristic peaks of PPy are observable in FTIR spectra of PPy/CNT composites and the intensities of PPy peaks are changed at different feeding mass ratios of PPy. However, the presence of CNT is not detectable because of its relatively high carbon amount and nonfunctionalized surface.

3.2. Different PPy morphologies in composites

Wire-, ribbon-, and sphere-like structures of PPy are obtained by using several surfactants and oxidizing agent and tailoring monomer concentrations [34]. Fig. 5a shows sphere-like nanostructures of PPy obtained by using FeCl_3 as an oxidant. Fig. 5c shows a very dense structure of cross-linked and non-functionalized CNT bundles due to PPy coverage when compared to pristine CNT shown in Fig. 5b. On the other hand, PPy starts to grow epitaxially on CNT surface acting as a template by increasing Py monomer concentration and a-layer-by-layer formation in some regions of Py:CNT = 2:1 composite is seen clearly in Fig. 5d. A lamellar structure is formed by self-assembly of PPy in CNT based composites due to the saturated monomer concentration [34]. Herein, higher amount of monomer causes to change in the reaction volume and growing direction of polymerization process and also conformational movement of chains, and thus a layer-by-layer formation is observed in some regions of composite. As it is seen in Fig. 5c, PPy are still in spherical form and the agglomeration of PPy nanospheres are observable in some parts due to the excess amount of Py monomer.

3.3. Synthesis of PPy/oxidized CNT composites

To provide better dispersion and appropriate interfacial adhesion between CNT and PPy, the surface of CNT was modified by oxidation process. Fig. 6 exhibits XRD patterns of oxidized CNT and its composites of Py:oxCNT = 1:1 and Py:oxCNT = 2:1.002 peak intensity values of oxidized CNT decrease significantly and get wider by increasing PPy amount in the composites since PPy has amorphous structure and weak diffraction peaks. Furthermore, crystallite size of CNT based composites calculated by using Debye Scherrer equations from XRD data shows that crystallite size values of pristine CNT and Py:oxCNT = 1:1 composite are 4.1 nm and 7.1 nm, respectively. After polymer coating on pristine CNT, crystallite size of Py:CNT = 1:1 composite becomes 5.7 nm. This difference stems from the attachment of oxygen groups on CNT surface that forms covalent bonds between a reactive pyrrole monomer and the surface of oxidized CNT bundles and thus increases the binding degree of PPy polymer.

Fig. 7 shows the Raman spectra of pristine CNT, oxidized CNT (oxCNT) and their composites by controlling the weight feed ratio of pyrrole and oxCNT as 1:1 and 2:1. Table 2 also represents the

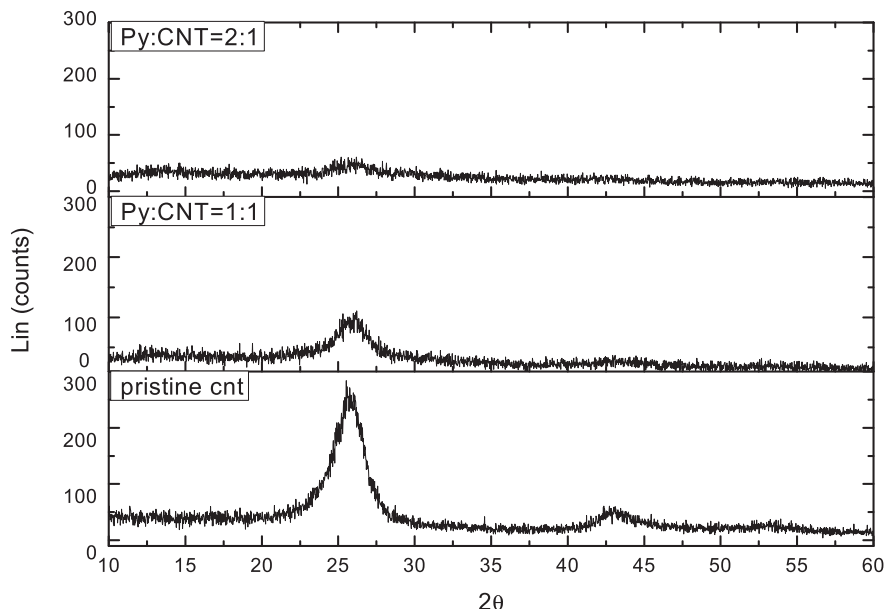


Fig. 2. XRD patterns of pristine CNT, Py:CNT = 1:1 and Py:CNT = 2:1 composites.

variations in I_D/I_G ratios of pristine CNT, oxCNT, Py:oxCNT = 1:1 and Py:oxCNT = 2:1. I_D/I_G ratio increases slightly after oxidation of pristine MWCNT since this process leads to the formation of defects in the structure of CNT because D band shows out of plane vibrations in the presence of structural defects and G band is attributed to in-plane vibrations of sp^2 bonded carbon atoms in aromatic rings and chains [35,36]. After PPy coating on the surface of oxidized CNT, I_D/I_G ratio continues to increase due to the covalent attachment of polymer onto CNT surface after oxidation process and also increasing oxygen functional group in CNT structure that result in a conversion of a small amount of sp^2 -to- sp^3 hybridized carbon. Also, 2D band intensity of PPy/oxCNT composites gradually decreases and this indicates an increase in the polymer thickness in the composites. When the I_D/I_G ratios of non-functionalized CNT and its composites are compared with the ones of functionalized samples, functionalized CNT-based composites have higher thickness and higher quantity of defects due to an increase of covalent bonds in

the presence of surface oxygen groups.

In order to detect the oxygen functional groups on the surface of CNT, FTIR analysis was conducted for each sample. After oxidation process, oxygen-containing functional groups are identified in the range of $2000\text{--}700\text{ cm}^{-1}$ in Fig. 8. The bands at 1040 cm^{-1} and 1150 cm^{-1} are assigned to C–O stretching in unsaturated hydroxyl groups [37]. The strong band at 1700 cm^{-1} is assigned to stretching vibration of C=O bonds in carboxylic acid groups while the weak band at 1615 cm^{-1} is due to the vibration mode of C=O in quinone groups on the surface of oxidized CNT [38]. In FTIR spectra of PPy/CNT composites, weak infrared peaks at $1780\text{--}1600\text{ cm}^{-1}$ corresponding to carbonyl groups indicate the presence of oxidized CNT in the structure.

Table 3 gives ^{13}C NMR chemical shifts and type of carbon environment of functionalized and non-functionalized of CNT composites with the feeding mass ratio of Py and CNT as 2:1. It is observed that the peak intensity of oxidized CNT/PPy composites in the region between 124 ppm and 133 ppm increases by approximately three times comparing to the ^{13}C NMR peak intensity of Py:CNT = 2:1 composite since the amount of PPy coated on the surface of oxidized CNT increases and this leads to an increase in C=C bond amount coming from PPy structure. Raman spectra of oxidized CNT composites in Fig. 7 also confirm an increase in sp^2 bonds because of oxidation process and PPy coating.

Fig. 9 shows SEM images of oxCNT, Py:oxCNT = 1:1 and Py:oxCNT = 2:1 composites. Oxidation process leads to the agglomeration of CNT bundles (Fig. 9a). After the dispersion of oxidized CNT in reaction mixture and the initiation of PPy polymerization, fluffy and porous structure formation is observed as seen in Fig. 9b. When compared to the results obtained by using

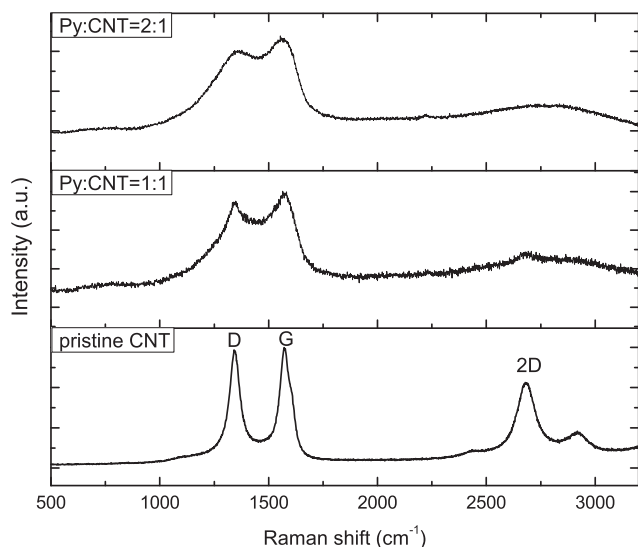


Fig. 3. Raman spectra of pristine CNT, Py:CNT = 1:1 and Py:CNT = 2:1 composites.

Table 1

The intensities of D and G bands, and I_D/I_G ratios of pristine CNT, Py:CNT = 1:1 and Py:CNT = 2:1 composites.

| Sample | D (a.u.) | G (a.u.) | I_D/I_G |
|------------------------|----------|----------|-----------|
| Pristine CNT | 6753 | 6776 | 1.00 |
| Py:CNT = 1:1 composite | 4102 | 4338 | 0.95 |
| Py:CNT = 2:1 composite | 9945 | 10,940 | 0.91 |

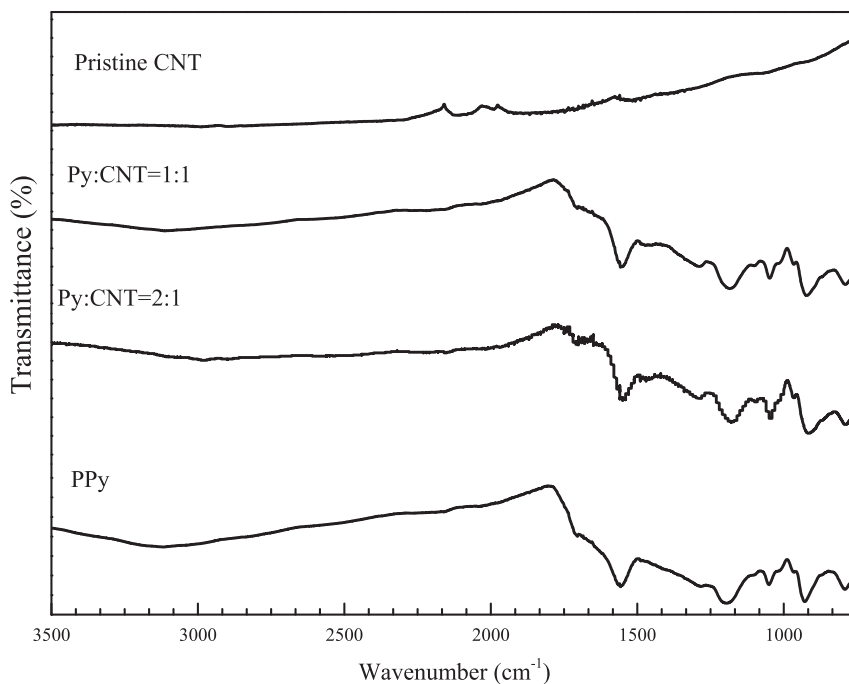


Fig. 4. FTIR spectra of pristine CNT, PPy, Py:CNT = 1:1 and Py:CNT = 2:1 composites.

pristine CNT, as pyrrole monomer concentration increases, PPy spheres do not aggregate on the surface of oxidized CNT and a layer-by-layer structure of PPy that is occurred due to high concentration of pyrrole monomer in composite is not detected in Fig. 9c and d. In addition, the thickness of CNT after oxidation and

polymer coating was measured by TEM. Fig. 10 exhibits TEM images of oxCNT, Py:oxCNT = 1:1 and Py:oxCNT = 2:1. The wall thickness of pristine CNT is about 4 nm whereas the thickness of CNT becomes 8 nm after coating by PPy in the feeding mass ratio of Py to oxCNT as 1:1. Then, CNT thickness increases up to 12 nm as Py

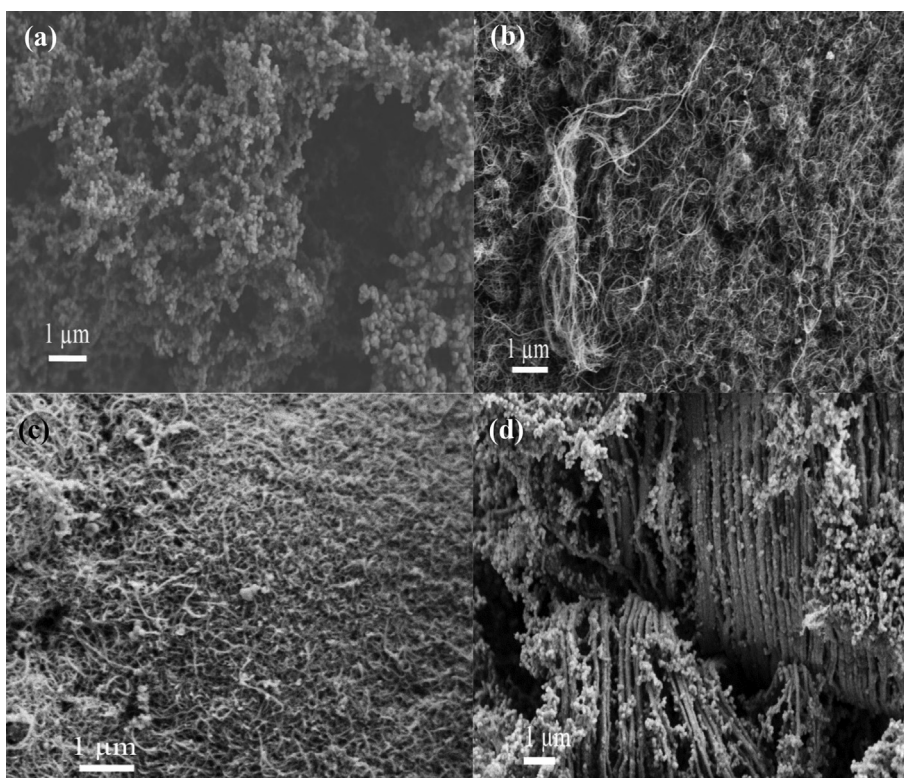


Fig. 5. SEM images of (a) pristine PPy, (b) pristine CNT, (c) Py:CNT = 1:1 composite and (d) Py:CNT = 2:1 composite.

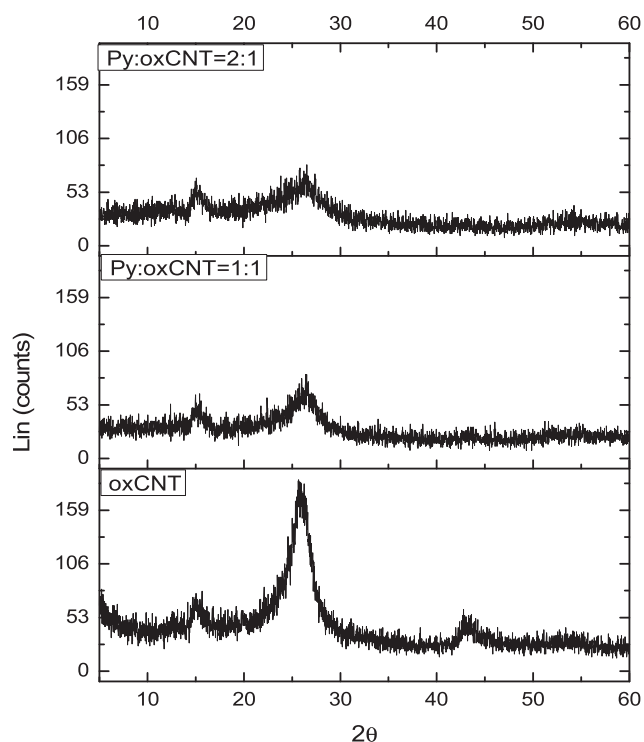


Fig. 6. XRD spectra of oxCNT and its composites of Py:oxCNT = 1:1 and Py:oxCNT = 2:1.

monomer is doubled in the reaction mixture. An increase in wall thickness is also proved by the comparison of I_D/I_G ratio in Fig. 7. Oxidation process of CNT surface prevents the agglomeration of PPy spheres and starts the layer-by-layer coating and thus gradual increase in wall thickness of CNT is observed.

EELS measures the elemental composition of CNT and its composites by measuring the energy loss during the interactions between incident electrons and CNT atoms [39]. EELS spectra in the carbon K-edge region, Fig. 11, are used to detect the changes in carbon content and observe the attachment of oxygen groups on the surface of pristine CNT, oxCNT, Py:oxCNT = 1:1 and

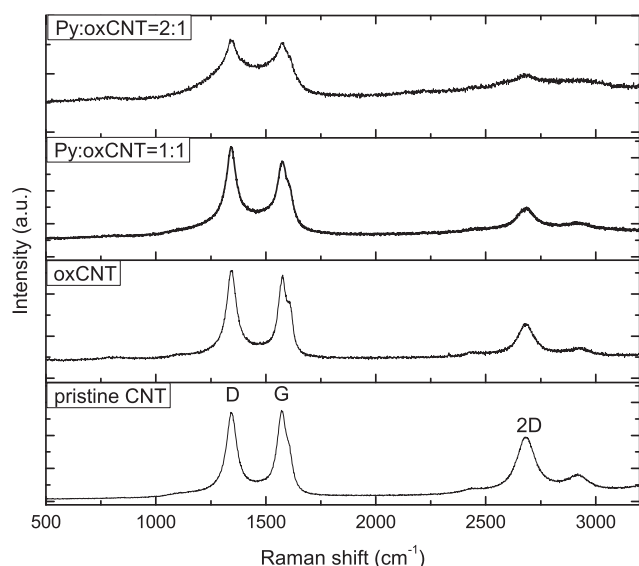


Fig. 7. Raman spectra of pristine CNT, oxCNT, Py:oxCNT = 1:1 and Py:oxCNT = 2:1.

Py:oxCNT = 2:1. The peak at 285 eV belongs to the 1s to the π^* states and the peak at around 291 eV shows the transitions from the 1s to the σ^* states. Quantitative analyses of C, O and N ratios by EELS measurement prove the changes in surface oxygen groups on the surface after oxidation and polymer coating that is given in Table 4. MWCNT contain 98.5% C and 1.5% O but oxCNT consist of 89.9% C and 10.4% O on its surface after oxidation process. Accordingly, the oxidation process changes the hydrophilic nature of MWCNT by increasing oxygen groups on the surface and thus provides homogenous dispersion in reaction media during polymerization. After coating the surface of MWCNT by PPy, Py:oxCNT = 1:1 composite has 89.4% C, 7.8% N and 2.8% O whereas Py:oxCNT = 2:1 composite contains 85.9% C, 13.5% N and 0.6% O due to an increase in PPy amount on the surface of CNT.

3.4. Surface area measurement

In surface area analysis, Brunauer–Emmett and Teller method (BET) provides specific surface area of CNT based samples and Barrett–Joyner–Halenda Method (BJH) is applied to measure pore radius (Mode $Dv(r)$) and pore volume in the mesopore and macropore ranges. BET surface area, BJH desorption pore radius and BJH desorption pore volume of CNT samples are given in Table 5. As PPy content increases in both pristine CNT and oxidized CNT composites, their BET surface area, BJH desorption pore radius and pore volume values drastically decrease due to the amorphous structure of PPy. Strong interactions cause localized adsorption which restricts the adsorbate to a specific site [40]. Chemical oxidation and polymer coating change the surface chemistry and thus a strong decrease is observed in the measured BET surface areas because of insufficient adsorption and incomplete monolayer coverage of the surface with molecules during analysis. These changes in pore radius and surface area affect directly the hydrogen adsorption capacities of CNT-based composites during IGA measurements.

3.5. Hydrogen sorption measurements by IGA

The IGA system uses the gravimetric technique to measure the magnitude and dynamics of hydrogen sorption on samples accurately. Fig. 12 shows hydrogen sorption curves of pristine CNT, PPy, oxCNT and Py:CNT = 1:1 composite in the range of 0–9000 mbar pressure at room temperature. IGA measurements indicate that pristine CNT, PPy, oxCNT and Py:CNT = 1:1 adsorb 0.46 wt.%, 0.14 wt.%, 1.03 wt.% and 1.66 wt.% hydrogen, respectively. Comparing the adsorption curves of these mentioned samples in Fig. 12a, one can observe that pristine samples of PPy and CNT have lower hydrogen uptake amounts whereas surface modification processes enhance hydrogen storage capacity significantly. An increase in hydrogen uptake values of oxidized CNT and PPy/CNT composites stems from the surface modification of CNT, the reduction in the pore size and an increase in unsaturated adsorption sites for hydrogen. During oxidation process, oxygen amount increases on the surface of CNT due to chromate ions and this leads to the increase in hydrogen uptake capacity. The comparable

Table 2

The intensities of D and G bands, and I_D/I_G ratios of pristine CNT, oxCNT, Py:oxCNT = 1:1 and Py:oxCNT = 2:1.

| Sample | D (a.u.) | G (a.u.) | I_D/I_G |
|----------------|----------|----------|-----------|
| Pristine CNT | 6753 | 6776 | 1.00 |
| oxCNT | 6309 | 6033 | 1.04 |
| Py:oxCNT = 1:1 | 8236 | 7212 | 1.14 |
| Py:oxCNT = 2:1 | 3996 | 3832 | 1.05 |

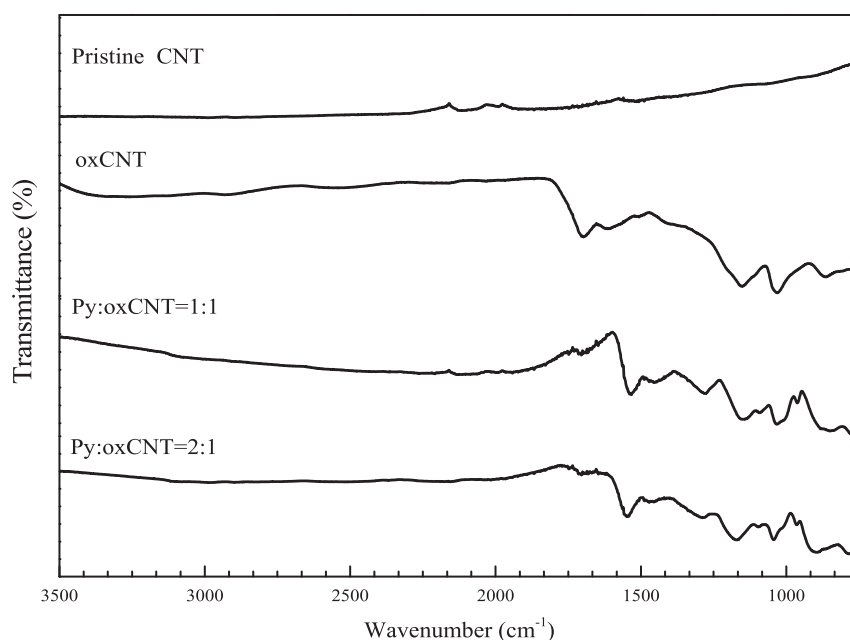


Fig. 8. FTIR spectra of pristine CNT, oxidized CNT, Py:oxCNT = 1:1 and Py:oxCNT = 2:1 composites.

Table 3

Chemical shifts of ^{13}C NMR spectra of Py:CNT = 2:1 and Py:oxCNT = 2:1 composites.

| Sample type | Chemical shift (ppm) | Peak intensity (a.u.) | Types of carbon environments |
|----------------|----------------------|-----------------------|------------------------------|
| Py:CNT = 2:1 | 109–130 | 11 | C=C |
| Py:oxCNT = 2:1 | 124–133 | 32 | C=C |

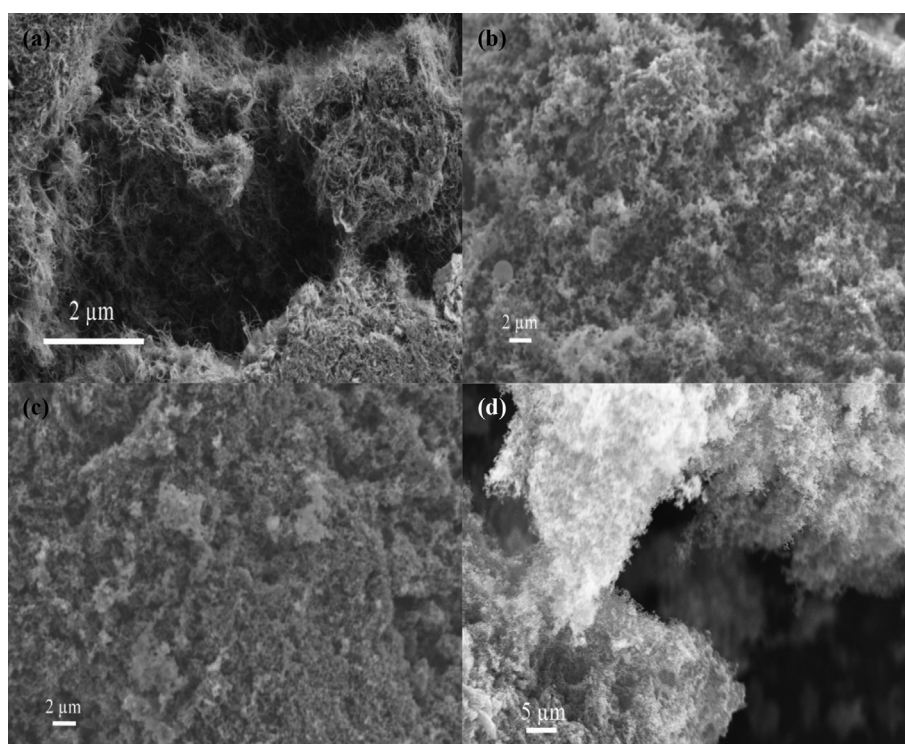


Fig. 9. SEM images of (a) oxCNT, (b) Py:oxCNT = 1:1 composite, (c) and (d) Py:oxCNT = 2:1 composite at different magnifications.

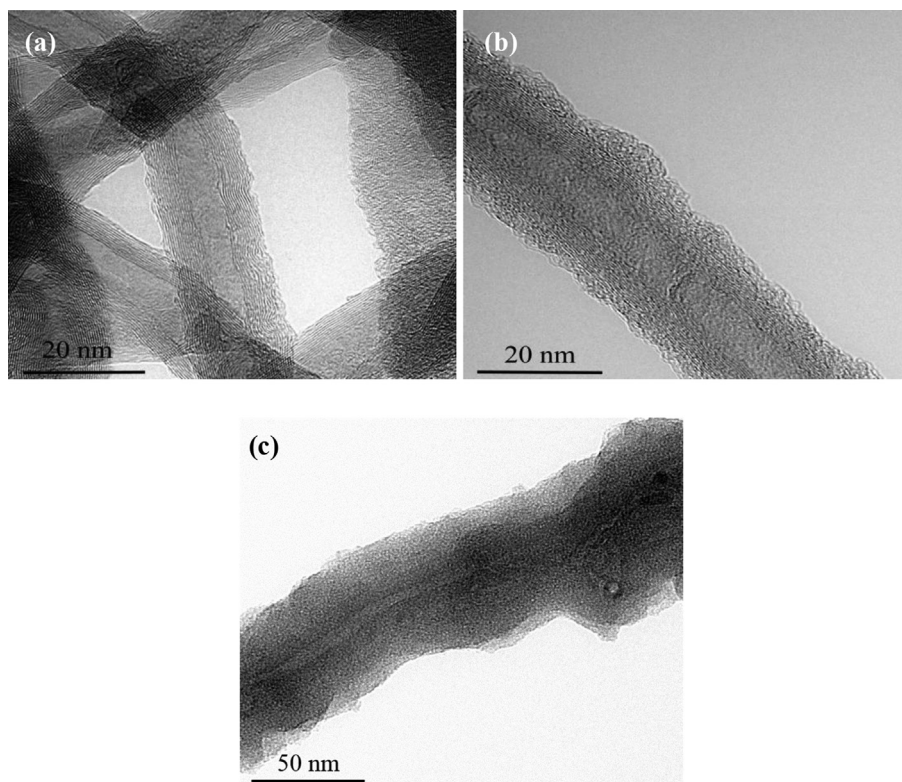


Fig. 10. TEM images of (a) oxCNT, (b) Py:oxCNT = 1:1 composite and (c) Py:oxCNT = 2:1 composite.

increase in hydrogen uptake value of Py:CNT = 1:1 composite originates from a decrease in pore size of CNT and an increase in the distance of CNT bundles [41]. In Fig. 12b, hydrogen adsorption/desorption isotherms of pristine CNT show good reversibility, and adsorbed hydrogen is released completely from the pores of CNT at room temperature due to relatively weak van der Waals bondings between hydrogen molecules and walls of CNT. In other words, complete reversibility and the absence of hysteresis loop between adsorption and desorption isotherms are observed since no chemical bonds are formed during physisorption. On the other hand, irreversible hydrogen sorption is observed in oxCNT and Py:CNT = 1:1 composite, as seen in Fig. 12c and d. Herein, adsorbed hydrogen is not released completely from the structure during

desorption and hysteresis loop is occurred because of accumulation of chemisorbed hydrogen atoms in the structure. This means that hydrogen is stored chemically in the pores of CNT and induces sp^3 -like hybridization and higher chemical potential is required to pull the adsorbed molecules out of their sites and obtain reversible adsorption/desorption isotherms [18]. Therefore, surface modification and polymer coating directly change the release behavior of adsorbed hydrogen from the pores. Furthermore, equilibrium time for each pressure point is adjusted as 3 h in the gravimetric sorption process. It is seen that adsorption kinetic of hydrogen is much faster than its desorption kinetic in the samples of oxCNT and Py:CNT = 1:1 at room temperature. Desorption process becomes faster at a pressure of zero at ultra high vacuum level (10^{-6} mbar) and thus sharp decrease is observed in the desorption isotherms of oxCNT and Py:CNT = 1:1 composite. The hysteresis loop of oxCNT is wider than one of Py:CNT = 1:1 because the desorption from oxCNT surface is prevented by high amount of oxygen functional groups.

It is also expected that hydrogen uptake capacity increases with increasing surface area [42,43]. However, CNT-based composites having lower BET surface area adsorb much more hydrogen atoms than the samples having higher BET surface area since hydrogen uptake for CNT is not only determined by surface area, pore size and chemical environment are also important parameters that affect hydrogen uptake. In our study, both polymer coverage and

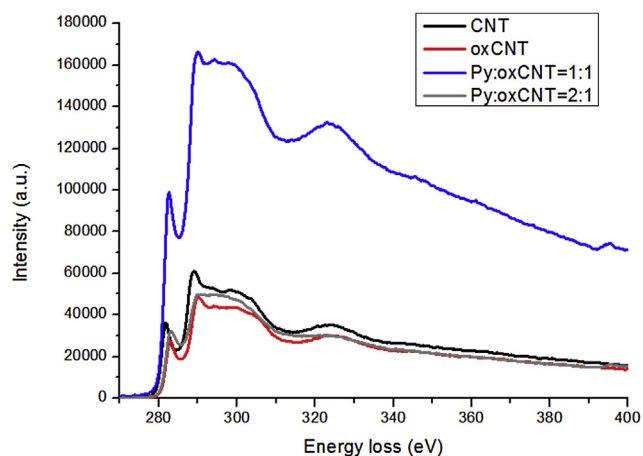


Fig. 11. EELS spectra of pristine CNT, oxCNT, Py:oxCNT = 1:1 and Py:oxCNT = 2:1.

Table 4
EELS elemental analysis results of CNT, oxCNT and their composites.

| Samples | C (%) | O (%) | N (%) |
|----------------|-------|-------|-------|
| Pristine CNT | 98.6 | 1.4 | – |
| oxCNT | 89.9 | 10.1 | – |
| Py:oxCNT = 1:1 | 89.4 | 2.8 | 7.8 |
| Py:oxCNT = 2:1 | 85.9 | 0.6 | 13.5 |

Table 5
Surface area analysis results of CNT and its composites.

| Sample | BET surface area (m ² /g) | BJH desorption pore radius (Å) | BJH desorption pore volume (cc/g) |
|----------------|--------------------------------------|--------------------------------|-----------------------------------|
| Pristine CNT | 198.5 | 149.5 | 1.4 |
| Py:CNT = 1:1 | 57.0 | 98.4 | 0.2 |
| Py:CNT = 2:1 | 25.8 | 88.1 | 0.3 |
| oxCNT | 107.8 | 138.3 | 0.7 |
| Py:oxCNT = 1:1 | 74.2 | 10.7 | 0.5 |
| Py:oxCNT = 2:1 | 67.8 | 8.4 | 0.4 |

oxidation process cause the reduction in pore size, and polymer coating forms new adsorption sites between the tube arrays in addition to the pores within CNT and thus the hydrogen storage properties of the produced composites are improved considerably.

4. Conclusions

Spherical PPy structures are synthesized on CNT surface by keeping identical mass ratio of pyrrole monomer and CNT. On the other hand, a layer-by-layer formation is observed at higher amount of pyrrole monomer in the structure of non-functionalized CNT composites. In order to figure out the effect of surface functionalization of CNT on the structural properties of PPy based composites, pristine CNT and functionalized CNT are coated by oxidative polymerization of PPy. After oxygen functionalization of CNT by acid treatment, homogeneous PPy coverage is observed and

the agglomeration of PPy spheres is prevented and thus wall thickness increases gradually by increasing the feeding mass ratio of pyrrole. Also, acid treatment leads to the reduction in the weight ratio of carbon and oxygen and the formation of hydrophilic surface. Increasing PPy amount causes to decrease the crystallinity of CNT composites and also BET surface area and BJH pore size. On the other hand, polymer coated CNT bundles form new adsorption sites between the tube arrays for hydrogen molecules. Therefore, hydrogen uptake values of CNT measured by IGA are improved significantly by surface oxidation and polymer coating and PPy coated CNT stores three times more hydrogen than pristine CNT at room temperature. Untreated CNT shows good reversibility in hydrogen adsorption/desorption isotherms due to the weak van der Waals interactions between hydrogen molecules. However, in the desorption isotherms of oxidized CNT and Py:CNT = 1:1 composite, hydrogen does not release from the pores and is chemically stored

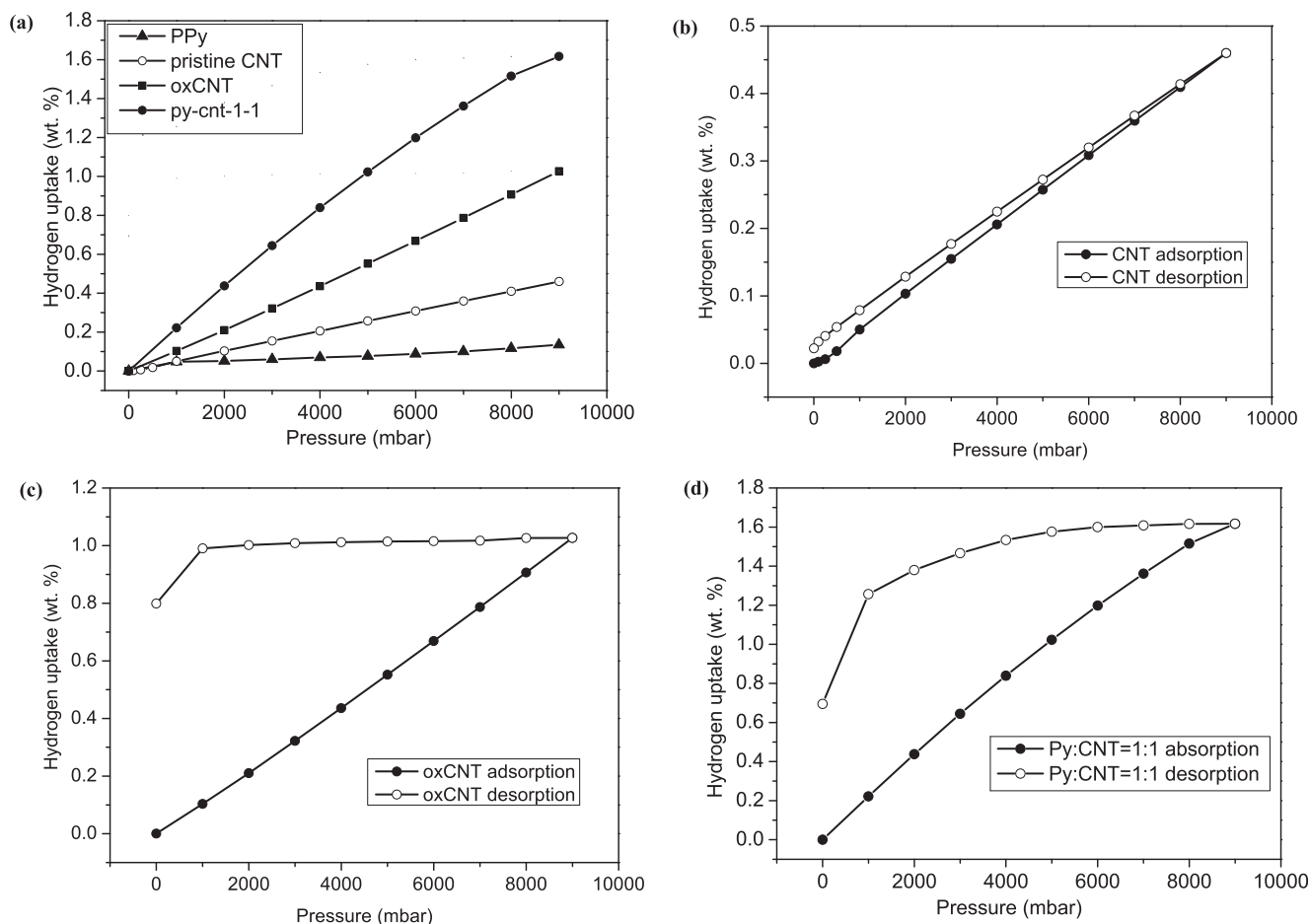


Fig. 12. (a) The comparison of adsorption isotherms of pristine CNT, PPy, oxCNT and Py:CNT = 1:1 composite, and hydrogen adsorption–desorption isotherms of (b) pristine CNT, (c) oxCNT and (d) Py:CNT = 1:1 composite.

in CNT structure and thus a hysteresis loop is occurred between adsorption and desorption curves. This originates from an increase in sp^2 bonds after oxidation process, defective and amorphous surfaces, and higher binding energies of chemisorbed hydrogen. Consequently, it is possible to enhance hydrogen storage properties of PPy/CNT composites by applying surface treatments. These modified composites become the most promising solid state systems for hydrogen storage due to their high volumetric/gravimetric capacity and fast adsorption kinetics at ambient conditions.

Acknowledgments

The authors would like to thank PhD student Mustafa Baysal for surface characterization and IGA measurements and laboratory specialist Ms. Burcin Yildiz for NMR characterization.

References

- [1] S.H. Lee, S. Lee, H.W. Ryu, H. Park, Y.S. Kim, J.H. Kim, Synthesis and in situ doping of highly conductive polypyrrole nanocomplexes with binary acids, *J. Polym. Sci. Polym. Chem.* 52 (2014) 2329–2336.
- [2] C. Cassagnol, P. Olivier, A. Ricard, Influence of the dopant on the polypyrrole moisture content: effects on conductivity and thermal stability, *J. Appl. Polym. Sci.* 70 (1998) 1567–1577.
- [3] U. Lange, N.V. Roznyatouskaya, V.M. Mirsky, Conducting polymers in chemical sensors and arrays, *Anal. Chim. Acta* 614 (2008) 1–26.
- [4] L. Nyholm, G. Nystrom, A. Mihanian, M. Stromme, Toward flexible polymer and paper-based energy storage devices, *Adv. Mater.* 23 (2011) 3751–3769.
- [5] J.H. Wu, Q.H. Li, L.Q. Fan, Z. Lan, P.J. Li, J.M. Lin, S.C. Hao, High-performance polypyrrole nanoparticles counter electrode for dye-sensitized solar cells, *J. Power Sources* 181 (2008) 172–176.
- [6] Z.H. Dong, Y.L. Wei, W. Shi, G.A. Zhang, Characterisation of doped polypyrrole/manganese oxide nanocomposite for supercapacitor electrodes, *Mater. Chem. Phys.* 131 (2011) 529–534.
- [7] S. Hara, T. Zama, S. Sewa, W. Takashima, K. Kaneto, Highly stretchable and powerful polypyrrole linear actuators, *Chem. Lett.* 32 (2003) 576–577.
- [8] J.H. Chen, Z.P. Huang, D.Z. Wang, S.X. Yang, W.Z. Li, J.G. Wen, Z.F. Ren, Electrochemical synthesis of polypyrrole films over each of well-aligned carbon nanotubes, *Synth. Met.* 125 (2001) 289–294.
- [9] H.C. Kang, K.E. Geckeler, Enhanced electrical conductivity of polypyrrole prepared by chemical oxidative polymerization: effect of the preparation technique and polymer additive, *Polymer* 41 (2000) 6931–6934.
- [10] H.B. Yildiz, S. Kiral, L. Toppare, Y. Yagci, K. Ito, Synthesis of conducting copolymers of thiophene capped poly(ethylene oxide) with pyrrole and thiophene, *Mater. Chem. Phys.* 100 (2006) 124–127.
- [11] B. Saner, S. Alkan Gursel, Y. Yurum, Layer-by-layer polypyrrole coated graphite oxide and graphene nanosheets as catalyst support materials for fuel cells, *Fuller. Nanotub. Carbon Nanostruct.* 21 (2013) 233–247.
- [12] L. Santos, P. Martin, J. Ghilane, P.C. Lacaze, J.C. Lacroix, Micro/nano-structured polypyrrole surfaces on oxidizable metals as smart electroswitchable coatings, *ACS Appl. Mater. Interfaces* 5 (2013) 10159–10164.
- [13] J. Liu, M.X. Wan, Studies on formation mechanism of polypyrrole microtubule synthesized by template-free method, *J. Polym. Sci. Pol. Chem.* 39 (2001) 997–1004.
- [14] S. Palaniappan, P. Manisankar, Rapid synthesis of polypyrrole nanospheres by greener mechanochemical route, *Mater. Chem. Phys.* 122 (2010) 15–17.
- [15] Y.Q. Han, X.T. Qing, S.J. Ye, Y. Lu, Conducting polypyrrole with nanoscale hierarchical structure, *Synth. Met.* 160 (2010) 1159–1166.
- [16] C. He, C.H. Yang, Y.F. Li, Chemical synthesis of coral-like nanowires and nanowire networks of conducting polypyrrole, *Synth. Met.* 139 (2003) 539–545.
- [17] B. Panella, L. Kossykh, U. Dettlaff-Weglikowska, M. Hirscher, G. Zerbi, S. Roth, Volumetric measurement of hydrogen storage in HCl-treated polyaniline and polypyrrole, *Synth. Met.* 151 (2005) 208–210.
- [18] M.U. Jurczyk, A. Kumar, S. Srinivasan, E. Stefanakos, Polyaniline-based nanocomposite materials for hydrogen storage, *Int. J. Hydrogen Energy* 32 (2007) 1010–1015.
- [19] G. Lota, K. Fic, E. Frackowiak, Carbon nanotubes and their composites in electrochemical applications, *Energy Environ. Sci.* 4 (2011) 1592–1605.
- [20] S.Y. Lee, S.J. Park, Effect of chemical treatments on hydrogen storage behaviors of multi-walled carbon nanotubes, *Mater. Chem. Phys.* 124 (2010) 1011–1014.
- [21] Z. Liu, Q. Xue, C. Ling, Z. Yan, J. Zheng, Hydrogen storage and release by bending carbon nanotubes, *Comput. Mater. Sci.* 68 (2013) 121–126.
- [22] W.Z. Huang, X.B. Zhang, J.P. Tu, F.Z. Kong, J.X. Ma, F. Liu, H.M. Lu, C.P. Chen, The effect of pretreatments on hydrogen adsorption of multi-walled carbon nanotubes, *Mater. Chem. Phys.* 78 (2003) 144–148.
- [23] I. Cabria, M.J. López, J.A. Alonso, Density functional study of molecular hydrogen coverage on carbon nanotubes, *Comput. Mater. Sci.* 35 (2006) 238–242.
- [24] A.C. Dillon, K.M. Jones, T.A. Bekkedahl, C.H. Kiang, D.S. Bethune, M.J. Heben, Storage of hydrogen in single-walled carbon nanotubes, *Nature* 386 (1997) 377–379.
- [25] G.G. Tibbetts, G.P. Meisner, C.H. Olk, Hydrogen storage capacity of carbon nanotubes, filaments, and vapor-grown fibers, *Carbon* 39 (2001) 2291–2301.
- [26] T.-M. Wu, S.-H. Lin, Characterization and electrical properties of Polypyrrole/Multiwalled carbon nanotube composites synthesized by in situ chemical oxidative polymerization, *J. Polym. Sci. Part B Polym. Phys.* 44 (2006) 1413–1418.
- [27] T.V. Vernitskaya, O.N. Efimov, Polypyrrole: a conducting polymer (synthesis, properties, and applications), *Usp. Khim.* 66 (1997) 489–505.
- [28] B. Saner, F. Okyay, Y. Yurum, Utilization of multiple graphene layers in fuel cells. 1. An improved technique for the exfoliation of graphene-based nanosheets from graphite, *Fuel* 89 (2010) 1903–1910.
- [29] S.P. Armes, Optimum reaction conditions for the polymerization of pyrrole by iron(III) chloride in aqueous-solution, *Synth. Met.* 20 (1987) 365–371.
- [30] A.C. Ferrari, J. Robertson, Interpretation of Raman spectra of disordered and amorphous carbon, *Phys. Rev. B* 61 (2000) 14095–14107.
- [31] N.G. Sahoo, Y.C. Jung, H.H. So, J.W. Cho, Polypyrrole coated carbon nanotubes: synthesis, characterization, and enhanced electrical properties, *Synth. Met.* 157 (2007) 374–379.
- [32] H. Murphy, P. Papakonstantinou, T.I.T. Okpalugo, Raman study of multiwalled carbon nanotubes functionalized with oxygen groups, *J. Vac. Sci. Technol. B* 24 (2006) 715–720.
- [33] M. Omastová, M. Trchová, J. Kovářová, J. Stejskal, Synthesis and structural study of polypyrroles prepared in the presence of surfactants, *Synth. Met.* 138 (2003) 447–455.
- [34] X.T. Zhang, J. Zhang, W.H. Song, Z.F. Liu, Controllable synthesis of conducting polypyrrole nanostructures, *J. Phys. Chem. B* 110 (2006) 1158–1165.
- [35] R. Saito, M. Hofmann, G. Dresselhaus, A. Jorio, M.S. Dresselhaus, Raman spectroscopy of graphene and carbon nanotubes, *Adv. Phys.* 60 (2011) 413–550.
- [36] A.C. Ferrari, Raman spectroscopy of graphene and graphite: disorder, electron–phonon coupling, doping and nonadiabatic effects, *Solid State Commun.* 143 (2007) 47–57.
- [37] U.J. Kim, C.A. Furtado, X. Liu, G. Chen, P.C. Eklund, Raman and IR spectroscopy of chemically processed single-walled carbon nanotubes, *J. Am. Chem. Soc.* 127 (2005) 15437–15445.
- [38] K. Gong, X. Zhu, R. Zhao, S. Xiong, L. Mao, C. Chen, Rational attachment of synthetic triptycene orthoquinone onto carbon nanotubes for electrocatalysis and sensitive detection of thiols, *Anal. Chem.* 77 (2005) 8158–8165.
- [39] A. Bougrine, A. Naji, J. Ghanbaja, D. Billaud, Purification and structural characterization of single-walled carbon nanotubes, *Synth. Met.* 103 (1999) 2480–2481.
- [40] S. Lowell, Joan E. Shields, Martin A. Thomas, Matthias Thommes, Characterization of Porous Solids and Powders: Surface Area, Pore Size and Density, Springer Science+Business Media, 2004, p. 74.
- [41] G. Yushin, R. Dash, J. Jagiello, J.E. Fischer, Y. Gogotsi, Carbide-derived carbons: effect of pore size on hydrogen uptake and heat of adsorption, *Adv. Funct. Mater.* 16 (2006) 2288–2293.
- [42] K.M. Thomas, Hydrogen adsorption and storage on porous materials, *Catal. Today* 120 (2007) 389–398.
- [43] A. Ghosh, K.S. Subrahmanyam, K.S. Krishna, S. Datta, A. Govindaraj, S.K. Pati, C.N.R. Rao, Uptake of H₂ and CO₂ by graphene, *J. Phys. Chem. C* 112 (2008) 15704–15707.